Eur J Nucl Med Mol Imaging (2007) 34:1240–1253
DOI 10.1007/s00259-006-0357-2

ORIGINAL ARTICLE

The basal ganglia matching tools package for striatal uptake semi-quantification: description and validation

Piero Calvini · Guido Rodriguez · Fabrizio Inguglia · Alessandro Mignone · Ugo Paolo Guerra · Flavio Nobili

Received: 31 May 2006 / Accepted: 9 December 2006 / Published online: 8 February 2007

Abstract
Purpose To design a novel algorithm (BasGan) for automatic segmentation of striatal ^{123}I-FP-CIT SPECT.
Methods The BasGan algorithm is based on a high-definition, three-dimensional (3D) striatal template, derived from Talairach's atlas. A blurred template, obtained by convolving the former with a 3D Gaussian kernel (FWHM= 10 mm), approximates striatal activity distribution. The algorithm performs translations and scale transformation on the bicommissural aligned image to set the striatal templates with standard size in an appropriate initial position. An optimization protocol automatically performs fine adjustments in the positioning of blurred templates to best match the radioactive counts, and locates an occipital ROI for background evaluation. Partial volume effect correction is included in the process of uptake computation of caudate, putamen and background. Experimental validation was carried out by means of six acquisitions of an anthropomorphic striatal phantom. The BasGan software was applied to a first set of patients with Parkinson's disease (PD) versus patients affected by essential tremor.
Results A highly significant correlation was achieved between true binding potential and measured ^{123}I activity from the phantom. ^{123}I-FP-CIT uptake was significantly lower in all basal ganglia in the PD group versus controls with both BasGan and a conventional ROI method used for comparison, but particularly with the former. Correlations with the motor UPDRS score were far more significant with the BasGan.
Conclusion The novel BasGan algorithm automatically performs the 3D segmentation of striata. Because co-registered MRI is not needed, it can be used by all nuclear medicine departments, since it is freely available on the Web.

Keywords ^{123}I-FP-CIT SPECT · Automatic VOIs · Parkinson's disease · Nigrostriatal system · Basal ganglia · Anthropomorphic brain phantom

P. Calvini
Department of Physics, University and INFN,
Genoa, Italy

G. Rodriguez · F. Nobili (✉)
Clinical Neurophysiology,
Department of Endocrinological and Metabolic Sciences,
University of Genoa, Genoa, Italy
e-mail: flaviomariano.nobili@hsanmartino.it

F. Inguglia
Department of Informatics and Information Sciences, University of Genoa,
Genoa, Italy

A. Mignone · U. P. Guerra
Nuclear Medicine Division, Ospedali Riuniti,
Bergamo, Italy

Introduction

Imaging of nigrostriatal endings by means of pre-synaptic radiopharmaceutical markers and single-photon emission computed tomography (SPECT)/positron emission tomography (PET) has gained increasing research and clinical attention in recent years. In a clinical setting, qualitative, visual analysis of striatal uptake is probably the most common approach for reporting of scans, although a categorization of visual analysis has been successfully applied in research work [1]. In a comparative study of this visual scoring system and a non-anatomical region of interest (ROI) method, the two systems yielded similar sensitivity and specificity in Parkinson's disease (PD), PD

dementia and Lewy body dementia versus either controls or patients with Alzheimer's disease (AD). However, the positive predictive value and the likelihood ratio were definitely better with the ROI method in the differentiation of patients with these parkinsonisms and AD patients [2]. As a matter of fact, the results derived from ROIs (especially if anatomically shaped with accuracy) have the potential to add value even in the clinical setting because they provide a continuous variable (rather than a categorical variable), which is more likely to express the wide clinical variability. Moreover, a continuous variable is more suitable for correlative analysis with other disease markers, such as those expressing the severity of motor impairment, for the assessment of disease progression [3] and the monitoring of neuroprotective treatments [4]. Finally, visual analysis suffers from inter-observer discrepancy in borderline conditions whereas an automatic method should be less affected by this drawback.

As a matter of fact, in nuclear medicine practice there is felt to be an increasing need for fully automatic procedures for three-dimensional (3D) semi-quantification of PET and SPECT tracer uptake in the striatum for a number of reasons. Firstly, the inter- and intra-observer variability of manual and semi-automatic ROI methods seems no longer to be acceptable either in clinical practice or, even more so, in research work. Secondly, both manual and geometric methods usually perform ROI drawing on a single slice or on a sum of adjacent slices and, consequently, they cannot provide information reflecting the 3D complexity of the whole striatal structure. Thirdly, longitudinal changes in uptake in an individual patient, whether that patient receives a putative neuroprotective agent or not, may be smaller than the variability deriving from manual method evaluations. Fourthly, it is mandatory that data from multicentre studies be obtained by the same approach.

The need for such automatic 3D methods for semi-quantification of nigrostriatal uptake has been felt since the end of the 1990s, and, in fact, some protocols have been proposed. The fuzzy c-means clustering approach was tested on a dynamic SPECT phantom derived from segmentation of the magnetic resonance (MR) image of an anthropomorphic brain phantom [5]. The same research group also proposed logistic discriminant parametric mapping to distinguish between PD patients and controls [6]. Koole et al. [7] prepared the segmentation of the striatum on the basis of MRI. Another approach utilized a striatal template built on the basis of a neuroanatomical atlas [8]. On the other hand, other authors built a reference template of the striatum from the scans of a series of normal subjects studied with ^{123}I-IBZM [9] or with ^{123}I-FP-CIT [10]. These methods have convincingly proven to be highly reproducible, to have no inter- or intra-observer variability since they are fully automatic, and to successfully discriminate patients with degenerative parkinsonism from normal subjects or from patients with essential tremor.

However, simplification and ease of use are required from a method conceived for widespread employment in as many nuclear medicine centres as possible. In this context, the methods based on MRI acquisition and co-registration cannot be easily used by all centres because a suitable 3D digital MRI scan of the patient is not routinely available. On the other hand, the methods based on the construction of a template from the scans of a relatively high number of normal subjects are hampered by the difficulty in collecting a sufficient number of scans of truly normal subjects. In this case, a camera-specific template should be prepared and, thus, diffusion and application of the method itself are rather limited. Those methods based on complex mathematical computations are even more problematic to apply in practice (and thus less likely to achieve widespread use). Given these considerations, the methods based on a template derived from a neuroanatomical atlas might be most easy to distribute and to utilize at a large number of centres.

Here we propose a fully automatic 3D method (named BasGan) for the unsupervised segmentation of the striatum on ^{123}I-FP-CIT SPECT scans. Validation on an anthropomorphic phantom and a first clinical application in patients with de novo PD in comparison with patients with essential tremor as controls are presented. The method is based on a template derived from the Talairach and Tournoux stereotactic neuroanatomical atlas. The software implementation runs on a Windows platform and can be freely downloaded from the Web [11]; thus, it can be easily applied and tested by most nuclear medicine centres worldwide.

Materials and methods

The templates

The proposed method is based on a high-definition 3D template of the striatum derived from Talairach and Tournoux's anatomical atlas [12] by means of a specific procedure. The pages of the atlas representing sagittal, coronal and axial sections of the right basal ganglia were scanned and the corresponding 2D images were obtained (pixel size=0.12 mm). From these high-resolution images, sections of the caudate nucleus and putamen were obtained by means of manual segmentation. The result consisted of 15 coronal, nine sagittal and ten axial sections of the right striatal complex. By using the coordinates supplied by the atlas, it was feasible to place these sections into the stereotactic space. Thus, a 3D template of the right striatal complex was derived as the binary map satisfying all requirements (i.e. shapes of all sections and relative

distances). As a by-product, an excellent degree of consistency was found among the various sections displayed in the atlas. Moreover, separate binary templates for the caudate nucleus and putamen were obtained for subsequent use. The voxel frame was the same for all templates, so that the binary template of the whole striatal complex was obtained by summing, voxel by voxel, the binary templates of the caudate nucleus and putamen. A template containing both caudate nucleus and putamen will be denoted in the following as a 'whole' template.

However, the resulting templates had too high a spatial resolution to be applied to SPECT images and, at the same time, suffered from some small-scale inaccuracies owing to the manual segmentation procedure. Thus, they were slightly smoothed and downsampled to a voxel size of about 0.7 mm. The result consisted of more regular templates having a spatial resolution high enough for the intended purpose. Figure 1 shows three views of the rendering of the whole 3D template obtained in this way. This template will be referred to as the 'high-resolution' template from now on; despite the smoothing, most of its binary character is preserved. Only a few voxels, namely those placed on the boundaries, take intermediate values between zero and unity. No overlap exists between the high-resolution template of the caudate nucleus and that of the putamen. The templates of the left striatal complex were obtained from the previous ones by mirroring.

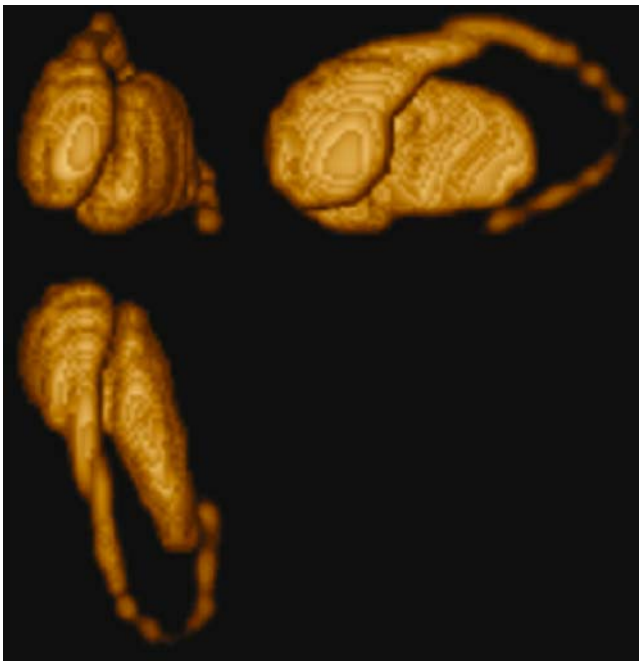

Fig. 1 Anterior, lateral and superior views of the rendering of the 3D template derived from Talairach and Tournoux's atlas. This template, referred to in the text as the high-resolution template, was obtained by smoothing the result of the manual segmentation procedure and by downsampling it to a voxel size of 0.7 mm from the original 0.12 mm voxel size

The ^{123}I-FP-CIT nigrostriatal activity distribution in SPECT images of subjects does not resemble the high-resolution template previously obtained since it is affected by the blur characteristic of this kind of imaging. Thus, 'low-resolution' templates were generated by applying a 3D Gaussian filter to the high-resolution ones. The chosen value for the full-width at half-maximum (FWHM) of the filter was 10 mm, consistent with the typical spatial resolution displayed by ^{123}I-FP-CIT SPECT images. Because of the blur, the low-resolution templates are not binary maps and their voxel values range between zero and one. In particular, values equal to one are still found in the deep core of the structure represented by the template and values equal to zero are found outside, at some distance from the nearest boundary. Three views of the rendering of the whole low-resolution template are shown in Fig. 2. Such a low-resolution template is meant to represent a realistic simulation of the activity distribution that a SPECT system usually recovers from the basal ganglia of a healthy subject.

The availability of independent caudate and putaminal templates can be exploited in two different ways. First, a set of whole low-resolution templates can be obtained by summing to the (low-resolution) caudate template a rescaled version of the putaminal template, obtained by multiplying by the same factor all voxel values of the original low-resolution putaminal template. In this way an adaptive model of activity distribution is obtained, tuned by the values given to that factor and able to fit all possibilities, from normalcy to severe putaminal impairment. As will be detailed in the following, the optimization program tries to place this adaptive template into a SPECT

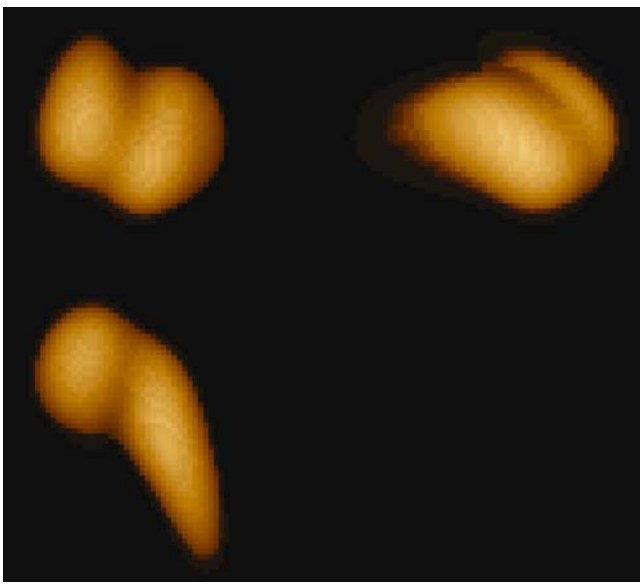

Fig. 2 Anterior, lateral and superior views of the rendering of the low-resolution template. It was obtained by applying a Gaussian filter (FWHM=10 mm) to the high-resolution template. The voxel sizes of the two templates are the same

image with the best approximation, and this tunability proves very effective in obtaining high-quality co-registrations. Second, as far as low-resolution templates are concerned, a relevant overlap between caudate nucleus and putamen exists, as can be observed by visual inspection of Fig. 2. Thus, in the whole low-resolution template (obtained by summing the caudate and putaminal templates with unit weights) the voxel values are the result of known contributions from the caudate and the putaminal compartments. An interpretation of such contributions in terms of probability will allow a partial volume effect (PVE) correction, as will be detailed in the next section.

The high-definition template, besides being the source for the blurred templates, is used in the last stage of the computation for monitoring purposes. We note that the FWHM of the Gaussian kernel applied in the filtering step can be changed and customized for a particular scanner and/or to a specific reconstruction protocol performance, if required.

The BasGan algorithm

The proposed method is based on the optimal positioning, automatically performed by the BasGan software, of the low-resolution templates (right and left ones, independently) on the input image, i.e. on the 3D ^{123}I-FP-CIT activity map of the patient. However, the input image must be scaled and positioned in a standard fashion for the automatic procedure to work properly. This preliminary step needs the orientation of the input image parallel to the bicommissural line (AC-PC position) and is the only manual intervention required from the user, who can achieve AC-PC orientation by means of a routine image visualization program before entering the software.

Alternatively, the user is prompted to choose suitable values of the yaw, roll and pitch angles which define the 3D rotation of the input image from the original orientation to the standard orientation of the atlas by means of a suitable graphical interface. All the rest runs automatically. The BasGan algorithm performs translations and scale transformation on the AC-PC aligned image in order to place the striata in a standard position and with a standard size. Independently of the original voxel size, the input image is isotropically resampled to a voxel size of 1.35 mm. Figure 3a shows an axial slice cut from the 3D activity map after these transformations. Then, an optimization protocol is activated which automatically performs fine tuning of the position and orientation of whole low-resolution templates on the standardized input image and locates an occipital ROI for background activity evaluation.

The optimizations for the positions of the two whole templates (right and left ones) are independent and are sequentially performed. The software seeks the optimal values of five parameters: translations along three mutually orthogonal directions in space (three parameters), rotation of the template around the head-to-feet axis (a yaw-type rotation, one parameter) and, lastly, tuning the putaminal contribution to the low-resolution whole template by means of the multiplicative factor previously introduced (one parameter). As already mentioned, the action of the latter parameter proves crucial in finding the optimal position of the template in the images of pathological subjects, in whom putamen activity can be drastically depressed in comparison to caudate uptake.

The algorithm, which seeks the best positioning of the whole templates in the image, performs rotations and subpixel translations. Then, interpolated voxel values are required and the resulting translated and/or rotated templates may suffer from some artefacts due to resampling if the sampling step of the original template is the same as that of the projected template. As a viable remedy for this problem, we decided to start from 0.7-mm sampled templates and to apply a compressive zoom (zoom factor 0.52=0.7/1.35) during the rotation/translation step in order to match the spatial sampling. In this way, 1.35-mm sampled templates are dynamically obtained, whose quality is largely independent of the shift and angle values.

In more detail, a void image is preliminarily prepared in voxelwise correspondence with the standardized input image. Then, for a set of five parameter values, a rotated and downsampled version of the low-resolution whole template is projected into the void image. Figure 3b shows

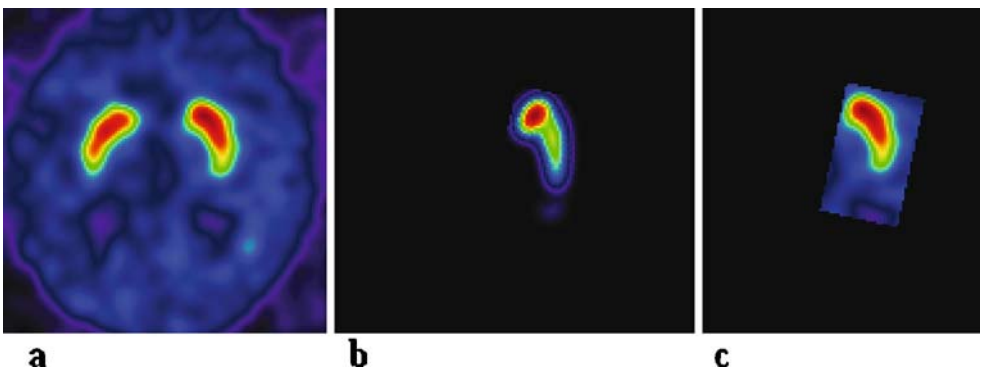

Fig. 3 **a** An axial section of a patient's activity map containing the striata. **b** An axial section of the 3D, low-resolution template suitably positioned by the algorithm for grabbing. **c** An axial section of the activity map grabbed by the template

an axial section of the void volume where the template is projected. A search for non-zero voxels in the (now nearly) void image localizes the position occupied in image space by the projected template and, therefore, permits grabbing in the input activity map of a subimage in spatial correspondence with the projected template (an axial section where the grabbing operated is shown in Fig. 3c). Last, the cross-correlation coefficient C is evaluated between the grabbed subimage, denoted by G, and the projected template, denoted by T (both T and G have the same number N of voxels and share the same voxel structure in space), according to the formula:

$$C_{T,G} = \frac{\sum_{i=1}^{N} \left(T_i - \overline{T}\right)\left(G_i - \overline{G}\right)}{\sqrt{\left[\sum_{j=1}^{N} \left(T_j - \overline{T}\right)^2\right]\left[\sum_{k=1}^{N} \left(G_k - \overline{G}\right)^2\right]}} \quad (1)$$

where the average value of T is given by

$$\overline{T} = \left(\sum_{i=1}^{N} T_i\right) \Big/ N \quad (2)$$

and an equivalent relation holds for G. For reasons of simplicity, in the previous relations, voxels are labeled by a single index according to a lexicographic ordering.

The optimization problem consists in finding the values of the five parameters which yield the maximum C and correspond to the best positioning of the low-resolution template upon the striatal activity of the input image. The cross-correlation coefficient has been chosen to drive the optimization of the co-registration since it is insensitive to a uniform background, as can be seen by inspecting the related formula. In fact, a uniform background added, for instance, to G affects the G terms in the differences by the same amount and, consequently, does not influence the value of C. The quality of the match is shown by suitable software which superimposes the boundaries of the high-definition templates onto the SPECT image. In the unlikely case of unsuitable positioning, the matching protocol can be restarted in a semi-automatic mode in order to fix some particular difficulties of the matching process.

The estimation of background activity is performed by means of a 3D occipital ROI which is automatically positioned by the software in the image. Such a 3D ROI was created as follows: Firstly, a 2D two-branch curved ROI was generated by dragging a 16-mm-diameter disk along 110° of a circle whose radius was 50 mm. The two-branch structure, designed with the aim of avoiding background evaluation in the inter-hemispheric fissure (often enlarged by atrophy), was generated by quitting the drag over 20° in the central position. Secondly, the 3D ROI was produced by stacking a 15-mm thickness of such 2D ROIs. The 3D ROI was placed by the algorithm at the upper level of the caudate heads.

Partial volume effect correction

The evaluation of uptake in caudate nuclei, putamina and background represents the next step after the optimal positioning of the templates in the input image. Since the spatial resolution offered by SPECT imaging is low in comparison with the fine details of the anatomical structures under investigation, the activity maps are affected by relevant partial volume effects (PVEs). In order to increase the accuracy of the semi-quantitative results provided by the proposed method, a correction for PVE is required. PVE correction was achieved by means of a technique which is rather similar to the approach proposed by Koole et al. [7] and is based on a five-compartment model: left and right caudate nuclei, left and right putamina, and background. Details and equations for PVE correction are given in the Appendix.

After performing PVE correction, putamen-to-background, caudate-to-background and putamen-to-caudate ratios and side to-side asymmetries are evaluated. Asymmetries are computed as $((L-R)/(L+R)\times 1/2)\times 100$, where L is the caudate or the putamen uptake in the left hemisphere and R is the corresponding value in the right hemisphere.

Phantom studies

To validate the algorithm, the anthropomorphic Alderson RSD phantom (designed ad hoc to reproduce the striatal morphology) was used. The 1,300 ml of the large brain volume (mimicking the cortex as a reference region) was first filled with half a litre of distilled water. Then, 1 ml of a 10-ml solution containing 6,500 kBq/ml of ^{123}I-iodide solutions was added to serve as background (cortical) activity. After carefully mixing the contents, the volume was entirely filled using distilled water. This procedure resulted in an activity concentration of approximately 5 kBq/ml.

The putamen was filled with 6 ml and the caudate with 5.5 ml of a 25-ml solution containing 40 kBq/ml. Care was taken to avoid air bubbles within each of the phantom compartments. After this reference SPECT acquisition, two acquisitions were performed soon afterwards by reducing the radioactive content of right striatum (filled with a solution of 26.7 kBq and then of 13.3 kBq/ml). At the end, the phantom was emptied and re-filled as for the first reference session, and a second reference acquisition was performed soon afterwards. Following this second reference SPECT acquisition, two acquisitions were performed by reducing the radioactive content of the two putamina (filled with a solution of 26.7 kBq and then of 13.3 kBq/ml). By this procedure, true BP values (BP=(Striatum−Background)/Background) were 7, 4.34 and 1.66 for filling with 40 kBq/ml, 26.7 kBq/ml and 13.3 kBq/ml, respectively.

Projections were acquired on a two-headed Millennium VG camera (GE) equipped with low-energy, high-resolution, parallel-beam collimators. For all tomographic acquisitions a step-and-shoot protocol was applied with a radius of rotation of 14 cm, and 120 projections evenly spaced over 360° were generated. Total counts ranged between 3 and 4 millions. The pixel size of the acquisition matrix was 2.4 mm, thanks to an electronic zoom (zoom factor=1.8) applied in the data collection phase. In the reconstruction phase also a digital zoom was used and the resulting images were sampled by cubic voxels with 2.33 mm sides.

Projections were processed by means of the ordered subsets expectation maximization (OSEM) algorithm (eight iterations, ten subsets) [13] followed by postfiltering (3D Gaussian filter with FWHM=8 mm). The OSEM algorithm included a proback pair accounting for collimator blur and photon attenuation. No compensation for scatter was performed. The 2D+1 approximation [14] was applied in the simulation of the space-variant collimator blur, while photon attenuation was modelled with the approximation of a linear coefficient uniform inside the skull and equal to 0.11 cm^{-1}.

The BasGan software was then applied and normalized uptake values were obtained as described in the previous section.

Correlation analysis was performed between true experimental BP and measured radioactive counts in caudate and putamen (the two sides being considered together).

Application to a first set of clinical data

For a first clinical application of the BasGan software, 13 consecutive drug-naive patients with de novo Parkinson's disease (PD) (1999-NINDS criteria) [15] were selected from the database of the laboratory. There were six males and seven females, aged 56–77 years (mean 66.8±6.8); the mean motor UPDRS score was 11.2±4.0; mean symptom duration was 9.8±4.9 months. The patients were affected by a prevalent akinetic-rigid syndrome. Dementia was excluded by Activities of Daily Living and Instrumental Activity of Daily Living standard questionnaires, and by neuropsychological evaluation.

Ten subjects with essential tremor diagnosed by a neurologist with expertise in movement disorders, according to the Movement Disorder Society criteria [16], were chosen as controls from the ^{123}I-FP-CIT SPECT database, the only criteria being a similar age to patients and absence of neuropsychoactive medication. Their scans were reported as normal by visual analysis, according to the conventional reporting criteria [1]. They comprised two males and eight females, with an age range of 47–72 years (mean 64.7±8.3).

In all patients, clinical follow-up for at least 1 year confirmed the diagnosis.

Both PD patients and controls underwent brain SPECT after i.v. administration of about 185 MBq of ^{123}I-FP-CIT (DaTSCAN, GE Healthcare, USA). SPECT was performed using the same camera and the same procedure as was used for the anthropomorphic phantom. Acquisition started between 180 and 240 min after injection. Patient preparation followed the recommendations of the European Association of Nuclear Medicine [17]. Total counts ranged between 2.5 and 3 millions.

The BasGan software was applied and volume of interest (VOI) values of normalized uptake in the striatum were computed.

ROI analysis

In order to compare BasGan results with a standard method widely used in clinical practice, a circular ROI was positioned on the head of the caudate nucleus and an elliptical ROI on the putamen by a nuclear medicine physician with expertise in ^{123}I-FP-CIT studies. A manual ROI for non-specific background uptake was positioned on the occipital lobe. The nuclear medicine physician (U.P.G.) was from another group and was blind to the clinical diagnosis. A slice was chosen where the putamen and the caudate could be best identified; then, the adjacent upper and lower slices were added to build a three-slice section. The number of voxels included in the circular caudate ROI was 180 (60 in each slice), in the elliptical putamen ROI, 210 (70 in each slice), and in the reference occipital ROI, 1,680 (560 in each slice). PVE correction was not applied to ROI analysis.

Statistics

For both BasGan and ROI data, abnormal normalized uptake values were considered in each patient when they were lower than the mean of controls −2 standard deviations. Comparison between values in PD and control groups was performed by the unpaired t test. Moreover, correlation (Pearson's r) was assessed between uptake values computed with either the BasGan or the ROI method and the motor UPDRS score.

Results

Phantom studies

The correct positioning of the VOIs on the striatum and on the occipital lobe was first visually verified in all the six phantom scans (example in Fig. 4). Numerical results of

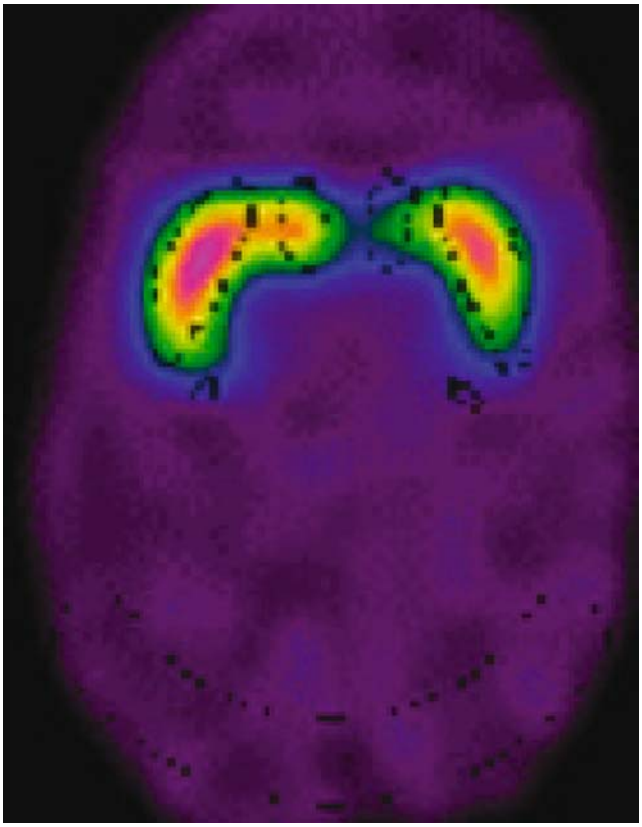

Fig. 4 Example of BasGan matching in phantom experimental session no. 2, where the striatal structures of the left side were filled with a 2/3 concentration of ^{123}I in comparison with the right-sided structures. The VOIs positioned by BasGan software are identified by *black dotted lines*

phantom studies are reported in Table 1. A highly significant correlation was achieved between true BP values and measured activity in both caudate (r=0.97) and putamen (r=0.97). Figure 5 shows the scatterplot of the correlation between measured and true BP values in the caudate and putamen considered together (mean correlation coefficient r=0.97).

Patient studies

As in the case of phantom studies, the correct positioning of the VOIs on the striatum and on the occipital lobe was first visually verified in all patients. Conventional ROI and BasGan VOI values in PD patients and controls are shown in Tables 2 and 3, respectively, and in Figs. 6 and 7. ^{123}I-FP-CIT uptake was significantly lower in all basal ganglia in the PD group in comparison to controls with both the ROI and the BasGan software method. An example of BasGan matching in a control subject and in a PD patient is given in Fig. 8. Tables 2 and 3 show the BP values of caudate and putamen, putamen-to-caudate ratios and asymmetries together with the p values for the statistical significance of differences between PD patients and controls obtained with the two methods. P values were almost always much higher with the BasGan than with the ROI method.

With the BasGan software, the BP values in PD patients were below the mean−2SD of controls in 13/13 cases for the putamen of the clinically more affected hemisphere, in 12/13 cases in the more affected caudate and in the less affected putamen and in 11/13 cases in the less affected caudate. The same values were obtained with the ROI method except in the case of the less affected putamen, which was lower than in controls in 9/13 cases.

As far as asymmetry values and ratios are concerned, values in PD patients were within the mean±2SD of controls in one case for caudate asymmetry and in one case for putamen asymmetry with the BasGan software, whereas putamen-to-caudate ratio was abnormally low in all patients. On the other hand, with the ROI method, values in PD patients were within the mean±2SD of controls in four cases for the ratio of the more affected site, in seven cases for the ratio of the less affected site, in four cases for caudate asymmetry and in six cases for putamen asymmetry.

Table 1 Uptake data of phantom studies normalized to the occipital reference ROI

	Left caudate		Right caudate		Left putamen		Right putamen	
Experimental session	Measured values	True BP values	Measured values	True BP values	Measured values	True BP values	Measured values	True BP values
1	6.04	7	6.37	7	5.93	7	5.60	7
2	6.37	7	4.83	4.34	5.71	7	4.28	4.34
3	6.26	7	2.74	1.66	6.04	7	2.30	1.66
4	6.75	7	6.75	7	6.09	7	5.92	7
5	6.26	7	6.09	7	4.93	4.34	5.10	4.34
6	5.94	7	6.09	7	2.79	1.66	2.62	1.66

True BP values according to phantom filling are also reported

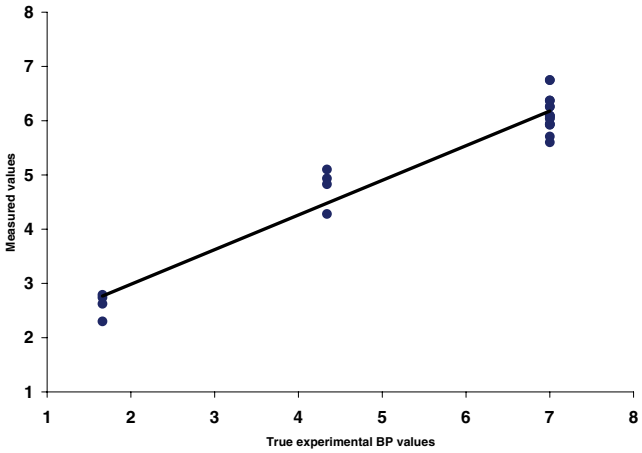

Fig. 5 Correlation (r=0.97) between experimental binding potential (BP) values (x axis) and measured values (y axis). Caudate and putamen of both sides are shown together

Finally, the r values of correlation with the motor UPDRS score were always higher with the BasGan than with the ROI method (Tables 2 and 3) (example in Fig. 9).

Discussion

This study shows that a fully automatic, unsupervised software for basal ganglia segmentation works properly in both experimental and clinical conditions and may be of value for quantification of basal ganglia uptake, especially in routine clinical work.

In fact, scans have been performed by means of a two-headed camera equipped with low-energy, high-resolution, parallel-beam collimators, one of the most available systems for ^{123}I-FP-CIT studies in nuclear medicine departments. The experimental and clinical validation with this kind of camera and the peculiarity that no further tool for VOI matching is required, make the BasGan package suitable for widespread diffusion and utilization. VOI positioning and numerical results are given in about 2 min after starting the program with a 512 RAM personal computer. In peripheral or basic nuclear medicine departments, without facilities of interfacing neuroradiological and physics departments, this may allow accurate quantification of ^{123}I-FP-CIT scans for diagnosis and follow-up purposes. On the other hand, in nuclear medicine centres of excellence, the BasGan package may be an alternative to other more sophisticated tools for ^{123}I-FP-CIT uptake quantification. In the latter setting it has the advantages of ease and speed of use, thus stimulating the preparation of a database of controls as well as multicentre studies. Another key feature of the BasGan software is that it is fully automatic, providing the scan is re-oriented according to the AC-PC line, as usually done before scan reporting. This can be achieved either before entering the image file in the package or by means of a tool within the package itself.

The phantom studies have consistently shown a satisfactory correlation between the true BP and the measured values during six experimental sessions. Despite the very good correlation achieved between measured and true BP experimental values in the phantom, the lowest filling resulted in an overestimation of measured counts. This overestimation might theoretically have been due to various factors, including over-correction produced by the PVE correction procedure and the non fully linear characteristics of the OSEM reconstruction algorithm [18]. Another possible explanation might be the experimental filling procedure, which did not include a washing step of basal ganglia chambers after acquisition with higher ^{123}I concentrations [19]. In fact, a decreasing filling order was followed during experimental sessions and this may account for the higher measured counts with lower filling concentrations, owing to the adhesion of ^{123}I remnants of previous higher concentrations to the plastic walls of the chamber. On the other hand, this phenomenon should not have been produced in PD patient studies, where a good correlation between basal ganglia uptake and the motor UPDRS score was found even with low or very low uptake values.

PVE correction is of major importance for proper functioning of the BasGan software and has been shown to be of paramount importance for estimation of the true BP of the basal ganglia [20, 21]. In a recent study [21] the importance of PVE correction procedures has been highlighted especially in borderline clinical conditions, such as the differentiation between patients with pre-clinical Lewy body dementia and AD patients.

Scatter correction can improve spatial resolution and can be obtained with a triple energy window method [22] or with other sophisticated methods applied as a pre-processing of the projections or at the reconstruction stage. In the present study, the BasGan software was applied to activity maps not corrected for scatter because of the need for operative simplicity, which reflects the working conditions of most nuclear medicine departments. This cannot be considered a limitation of the software itself, but rather is simply a consequence of routine operative conditions. Furthermore, PVE correction appears to be far more important than both attenuation and scatter correction for clinical purposes [20].

The method of maximization of the cross-correlation coefficient was chosen to co-register the template to SPECT data. The choice was intended to take into consideration the wide variability of data commonly acquired in clinical practice, ranging from normal subjects to patients with very low basal ganglia uptake, which renders distinction from background difficult. In fact, the cross-correlation coeffi-

Table 2 Background-normalized uptake values of the striatum, putamen-to-caudate ratio and asymmetry values in control subjects and PD patients obtained with the conventional ROI method used as reference

	CTR caudate	PD caudate		CTR putamen	PD putamen		CTR ratio	PD ratio		CTR	PD	CTR	PD
		More affected hemisphere	Less affected hemisphere		More affected hemisphere	Less affected hemisphere		More affected hemisphere	Less affected hemisphere	Caudate asymm	Caudate asymm	Putamen asymm	Putamen asymm
Mean	2.67	0.97	1.08	2.44	0.61	0.86	0.90	0.66	0.80	1.5	10.9	−0.6	30.2
SD	0.59	0.34	0.35	0.70	0.15	0.33	0.08	0.15	0.18	6.4	18.4	8.8	19.8
Coeff. of variation	0.22	0.35	0.32	0.29	0.25	0.38							
P value		7.5^{-11}	3.5^{-10}		1.34^{-10}	9.8^{-9}		4.1^{-7}	0.02		0.07		0.002
Mean−2SD	1.49			1.02			0.74			−11.3/ 14.3		−18.2/ 17.0	
PD patients within mean±2SD of CTR[a]		1	2		0	4		4	7		4		6
True overlap[b]		1	2		0	1		1	4		10		6
UPDRS correlat. *r* value		−0.29	−0.22		0.04	−0.32		0.44	−0.22		0.14		−0.40

CTR controls, *PD* Parkinson's disease patients, *ratio* putamen-to-caudate ratio, *asymm* asymmetries

[a] Number of PD patients with the corresponding value within the control mean±2 standard deviations

[b] Number of PD patients with values in between the minimum and the maximum of corresponding values of controls

Table 3 Background-normalized uptake values of the striatum, putamen-to-caudate ratio and asymmetry values in control subjects and PD patients obtained with the BasGan software

	CTR caudate	PD caudate		CTR putamen	PD putamen		CTR ratio	PD ratio		CTR	PD	CTR	PD
		More affected hemisphere	Less affected hemisphere		More affected hemisphere	Less affected hemisphere		More affected hemisphere	Less affected hemisphere	Caudate asymm	Caudate asymm	Putamen asymm	Putamen asymm
Mean	4.21	1.99	2.35	3.59	0.69	1.21	0.85	0.34	0.50	−1.1	16.9	−3.6	51.0
SD	0.67	0.64	0.78	0.66	0.29	0.62	0.06	0.07	0.14	3.5	20.9	6.3	29.1
Coeff. of variation	0.15	0.32	0.33	0.18	0.42	0.51							
P value		6.9^{-11}	1.8^{-8}		6.2^{-16}	6.7^{-12}		10^{-21}	4^{-11}		0.007		4.6^{-6}
Mean−2SD	2.86			2.27			0.72			−8.1/ 5.9		−16.2/ 9.0	
PD patients within mean±2SD of CTR		1	2		0	1		0	0		1		1
True overlap		0	2		0	0		0	0		0		2
UPDRS correlat. *r* value		−0.51	−0.34		−0.47	−0.51		−0.1	−0.56		0.28		−0.31

Footnotes to Table 2 apply

cient values are independent of the global counts of SPECT examination and, more importantly, of (uniform) background uptake, as previously remarked in the section Materials and methods [see Eqs. (1) and (2)] [23].

Comparison between the ROI method and the BasGan package

Background-normalized ^{123}I-FP-CIT uptake values were higher when applying the BasGan package than when using the ROI method. Conversely, the coefficients of variation were much lower using the former in control patients, but higher in both the putamina of PD patients. This means that the variance of values was lower in controls with the BasGan package, thus identifying a more homogeneous group. However, variance was higher in the putamen of PD patients, and thus the BasGan package was able to differentiate the different degrees of nigrostriatal involvement better than could the ROI method.

If we consider the putaminal ^{123}I-FP-CIT uptake of the clinically more affected hemisphere as the most sensitive index for distinction of PD patients from controls, both the ROI and the BasGan method had a 100% sensitivity. However, the differences between the two groups were statistically far more significant with the BasGan tool than with the ROI method. Moreover, if the caudate-to-putamen ratio and side-to-side asymmetries are considered, sensitivity was definitely higher when applying the BasGan tool than when using the ROI method (100% vs 69% and 46% sensitivity for caudate-to-putamen ratio of the more and the less affected hemisphere, respectively; 92% vs 69% sensitivity for caudate asymmetry; 92% vs 54% sensitivity for putamen asymmetry). As shown in Tables 2 and 3, the overlap between patients and controls was definitely higher when considering the putamen-to-caudate ratio and asymmetry values computed with the ROI method. This result highlights the ability of the BasGan method to better differentiate uptake values in PD patients and controls, and may be extremely relevant in borderline clinical conditions.

Finally, the higher clinical significance of the BasGan method was shown by the higher correlation coefficient achieved with the motor UPDRS score in comparison with the ROI method. The correlation between the motor UPDRS score and the striatal uptake is generally reported to be moderate, and it is statistically significant within a wide range of values [24]. As a matter of fact, within the present narrow range of motor UPDRS score (from 5 to 21) we found such a correlation when using the uptake values obtained with the BasGan tool, but not when using the ROI values.

The better performance of the BasGan package can be explained by several factors. First, it operates a PVE correction, which is not performed by a simple ROI method

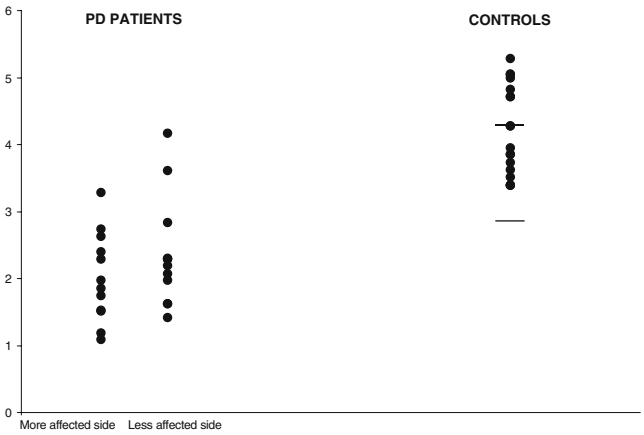

Fig. 6 Scatterplot of individual values obtained with the BasGan software in the caudate in controls (mean and −2SD bars are shown) and in PD patients. An overlap is seen in two instances for the less affected caudate and in one instance for the more affected caudate

and which has been shown to greatly improve differentiation between groups [21]. Second, the entire volume of the basal ganglia is considered, and this can magnify differences between patients and controls and among patients themselves. For instance, the caudate tail is included in the BasGan template, but it is usually missed by the ROI method. Third, boundary definition of basal ganglia is based on Talairach's anatomical shapes, whereas it is just approximated by the ROI method. Fourth, and most important, in some PD patients the putamen uptake value of the more affected hemisphere is so low that its boundaries cannot be safely identified by the ROI method and an elliptical ROI can only be positioned with reference to the contralateral one. The BasGan tool, as well as other methods based on anatomical shapes, defines striatal boundaries even in those cases with very low uptake values. Such a solution has been proven to be adequate both by experimental phantom validation and by the better identification of this sample of PD patients.

Limitations

The most obvious limitation is that the basal ganglia shape and dimensions are not identical among individuals and thus a template based on Talairach's atlas represents an approximation. Talairach's brain predates modern digital scans and is not representative of the general population. The Montreal Neurological Institute has produced a set of MR images which are widely used to map images into a space similar to, but different from, Talairach's space. Even though the MNI templates have been officially adopted by the International Consortium for Brain Mapping, the fact remains that they do not constitute an atlas. In contrast, the Talairach atlas is currently considered by the neurological community as the standard reference for locating structures and functional areas [25]. Because of the relatively low spatial resolution of SPECT imaging and the blur effect of collimators, it is unlikely that shape or dimension mismatch of the basal ganglia leads to substantial errors in the evaluation of ^{123}I-FP-CIT uptake. As already mentioned in the Introduction, this limitation is overcome by the methods based on the MRI of each individual [7].

It might be argued that another limitation resides in the 3D coordinate positioning of the basal ganglia in each subject. However, this has been largely overcome by the five-parameter optimization procedure which automatically finds the best positioning of the template independently on each striatum. Thus, the particular orientation of both striata of each individual is matched to a satisfactory level of accuracy by template rotations and translations. Moreover, the fifth parameter (the "putamen-depressing parameter") usually permits satisfactory positioning of the template even in patients with very low uptake.

The BasGan software provides a mean uptake value within a VOI and does not permit voxel-based analysis, which is allowed by other methods, such as statistical parametric mapping (SPM) [26] and brain registration and analysis of SPECT studies (BRASS) [27]. Although these methods have been successfully applied to individual analysis [28] and can detect significant uptake changes limited to a portion of the basal ganglia, a mean uptake value for the whole of either the caudate or the putamen should satisfy the majority of clinical and research needs. Furthermore, application of the aforementioned methods requires a reference template containing control subjects acquired with the same gamma camera and collimators, which is not needed by the BasGan software.

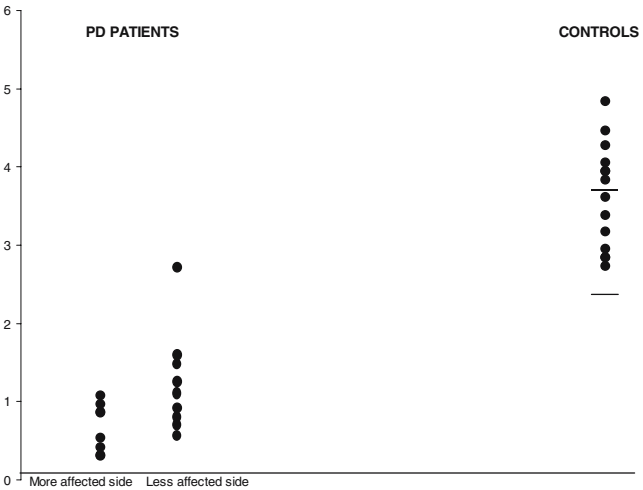

Fig. 7 Scatterplot of individual values obtained with the BasGan software in the putamen in controls and in PD patients. An overlap is seen in one instance in the less affected caudate

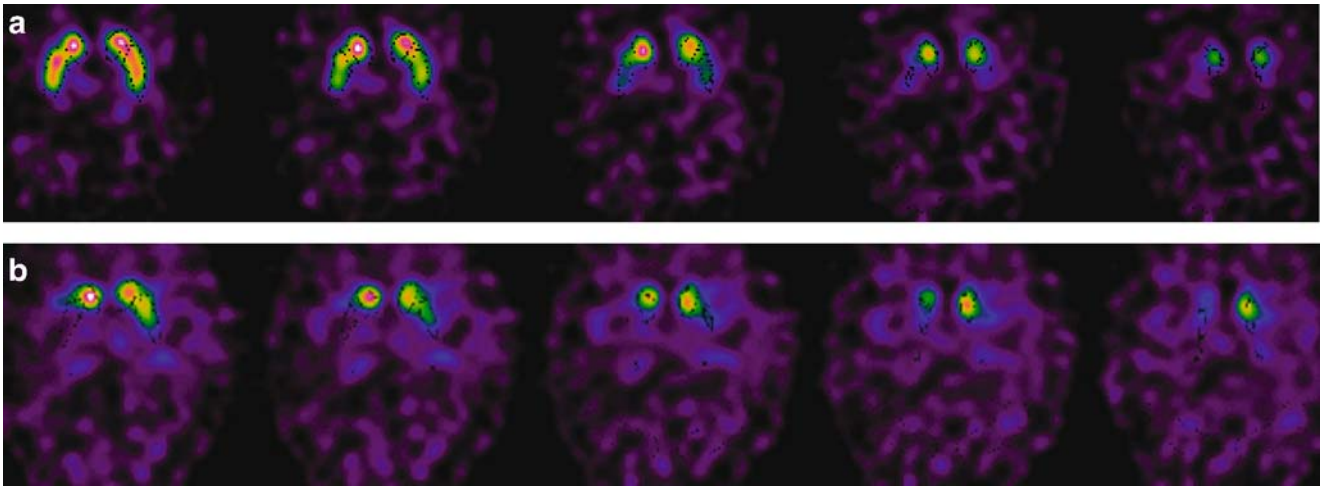

Fig. 8 Five transaxial slices showing a BasGan matching example in (**a**) a control subject with essential tremor and in (**b**) a PD patient. The VOIs positioned by BasGan software are identified by *black dotted lines*

Conclusion

The automatic BasGan software has been shown to work properly in the unsupervised identification of ^{123}I-FP-CIT uptake both in a phantom experimental study and in a first set of patients, in whom the results were more clinically consistent than those obtained with a conventional ROI method. The main advantages of this software are that it works without needing a patient's digital MRI and that it is freely downloadable from the web [11].

Acknowledgements The BasGan software has been partially developed with the financial support of GE-Healthcare, Italian Division (Milan), which has also supported translation of the BasGan package instruction manual on the Web from the original Italian version into English. We thank Dr.Enrico Seccamani and Dr. Vincenzo Orlando of GE for following the project since its inception.

Our thanks also go to Dr. Nicola Girtler and Dr. Andrea Brugnolo of the Clinical Neurophysiology Division in Genoa for performing the neuropsychological evaluation in PD patients and to Dr. Arnoldo Piccardo and Dr. Silvia Morbelli at the Nuclear Medicine Dept. of the University of Genoa for acquiring SPECT scans in PD patients and controls.

Finally, we wish to thank Elizabeth Cotton for English editing.

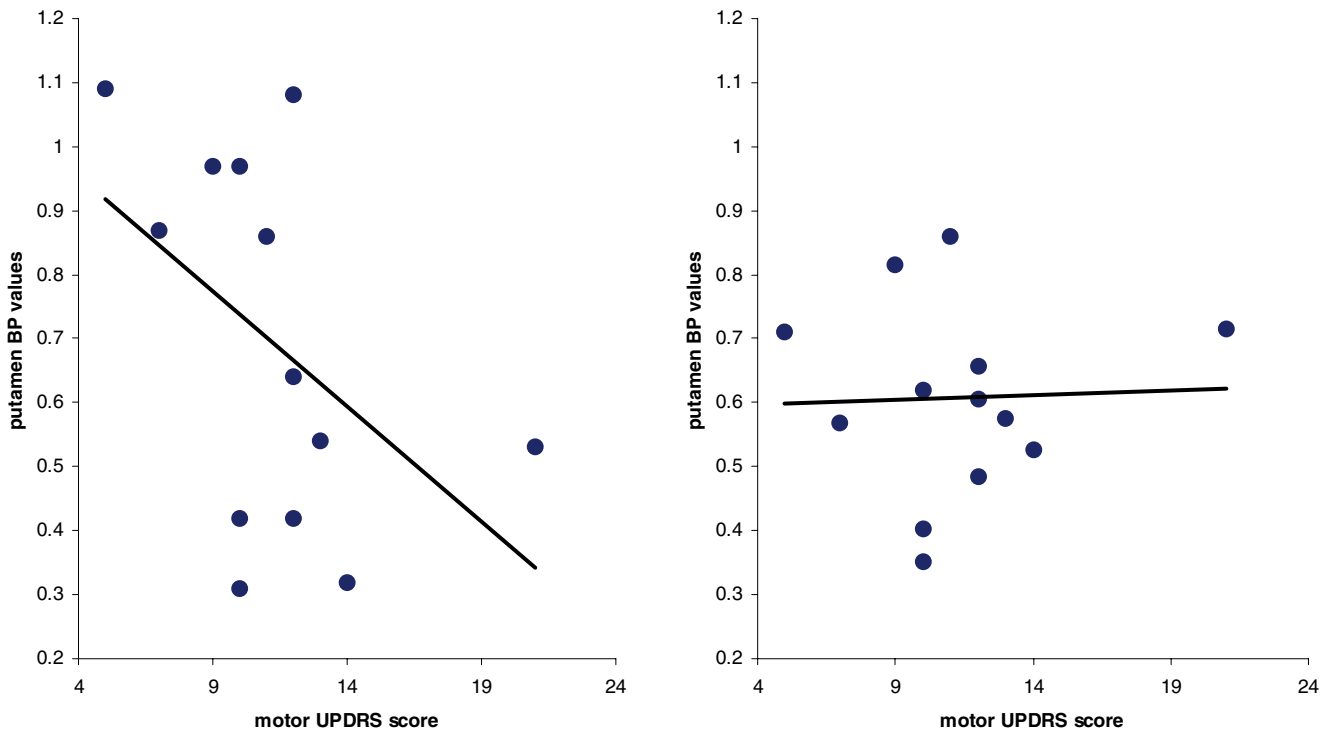

Fig. 9 Scatterplot of correlation between motor UPDRS score (*x* axis) and BP values in the more affected putamen (*y* axis) in PD patients, as achieved with the BasGan software (*left side*; $r=-0.47$, $p<0.05$) and the ROI method (*right side*; $r=0.04$, p NS)

Appendix: PVE correction

Activity concentration is considered to be uniform within each compartment. We suppose that PVEs do not produce appreciable cross-talk effects between the left and the right side in activity evaluation and, therefore, that each side can be processed independently.

Relative to one side (e.g. right side), we denote by $\widetilde{C}$, $\widetilde{P}$ and B the unknown activity concentrations in the caudate nucleus, putamen and background compartments, respectively. Activity concentration B of the background can be easily evaluated by the ratio of all counts contained in the background ROI over the number of voxels of the ROI itself, since the background ROI is not appreciably affected by PVEs. The value of B is the same for both sides. The problem consists in finding the values of $\widetilde{C}$ and $\widetilde{P}$ relative to non-overlapping compartments on the basis of the information derived from a PVE-affected activity map, where the counts contained in a voxel may contain contributions from different compartments.

We denote by c_i, p_i and b_i (i=1,..., N), respectively, the low-resolution templates of the overlapping compartments caudate nucleus, putamen and background as projected into the image space at the optimal positioning (indeed, index i explores all grabbed voxels in the input activity map, i.e. all voxels targeted by the projection). Moreover, we point out that the background compartment b_i (i=1,..., N) must not be confused with the background ROI used to estimate B. After projecting the templates c_i and p_i into image space, the background compartment b_i is obtained as the complement to unity of the sum c_i+p_i over the range of all grabbed voxels. Thus the following relation holds:

$$c_i + p_i + b_i = 1 \ (i = 1, \ldots, N) \tag{3}$$

which can be given the probabilistic interpretation that the grabbed voxel i may contain counts from caudate compartment with probability c_i, from putaminal compartment with probability p_i and from background with probability b_i. Thus, the PVE-affected data v_i (i.e. the grabbed voxels of the activity image) contain contributions from the three compartments according to the following relation:

$$v_i = \widetilde{C}\, c_i + \widetilde{P}\, p_i + B\, b_i. \tag{4}$$

Thanks to the hypothesis that the background receptors are uniformly spread all over the brain, including the striatum, one is interested in the activity concentrations C and P given by:

$$C = \widetilde{C} - B\,;\; P = \widetilde{P} - B. \tag{5}$$

Finally, the set of equations connecting the experimental data v_i with the unknowns C and P are:

$$v_i - B = C\, c_i + P\, p_i \ (i = 1, \ldots, N), \tag{6}$$

whose solution can be estimated by solving the following least-squares problem:

$$\sum_{i=1}^{N} (v_i - B - C\, c_i - P\, p_i)^2 = \text{minimum}. \tag{7}$$

In this way one obtains PVE-corrected estimates for the activity concentrations C and P, from which the ratios C/B and P/B can be derived, respectively denoted as the caudate and putaminal values.

References

1. Benamer TS, Patterson J, Grosset DG, Booij J, de Bruin K, van Royen E, et al. Accurate differentiation of parkinsonism and essential tremor using visual assessment of ^{123}I-FP-CIT SPECT imaging: the ^{123}I-FP-CIT Study Group. Mov Disord 2000;15:503–10.
2. O'Brien JT, Colloby S, Fenwick J, Williams ED, Firbank M, Burn D, et al. Dopamine transporter loss visualized with FP-CIT SPECT in the differential diagnosis of dementia with Lewy bodies. Arch Neurol 2004;61:919–25.
3. Chouker M, Tatsch K, Linke R, Pogarell O, Hahn K, Schwarz J. Striatal dopamine transporter binding in early to moderate advanced Parkinson's disease: monitoring of disease progression over 2 years. Nucl Med Commun 2001;22:721–5.
4. Marek K, Seibyl J, Shoulson I. Dopamine transporter brain imaging to assess the effects of pramipexole vs levodopa on Parkinson disease progression. JAMA 2002;287:1653–61.
5. Acton PD, Pilowsky LS, Kung HF, Ell PJ. Automatic segmentation of dynamic neuroreceptor single-photon emission tomography images using fuzzy clustering. Eur J Nucl Med 1999;26:581–90.
6. Acton PD, Mozley PD, Kung HF. Logistic discriminant parametric mapping: a novel method for the pixel-based differential diagnosis of Parkinson's disease. Eur J Nucl Med 1999;26:1413–23.
7. Koole M, Laere KV, De Walle RV, Vandenberghe S, Bouwens L, Lemahieu I, et al. MRI guided segmentation and quantification of SPECT images of the basal ganglia: a phantom study. Comput Med Imaging Graph 2001;25:165–72.
8. Habraken JBA, Booij J, Slomka P, Sokole EB, van Royen EA. Quantification and visualization of defects of the functional dopaminergic system using an automatic algorithm. J Nucl Med 1999;40:1091–7.
9. Radau PE, Limke R, Slomka PJ, Tatsch K. Optimization of automated quantification of ^{123}I-IBZM uptake in the striatum applied to parkinsonism. J Nucl Med 2000;41:220–7.
10. Koch W, Radau PE, Hamann C, Tatsch K. Clinical testing of an optimized software solution for an automated, observer-independent evaluation of dopamine transporter SPECT studies. J Nucl Med 2005;46:1109–18.
11. http://www.disi.unige.it/person/InguglaF/BasGan/
12. Talairach J, Tournoux P. Co-planar stereotaxic atlas of the human brain. New York: Thieme Medical, 1988.
13. Hudson HM, Larkin RS. Accelerated image reconstruction using ordered subsets of projection data. IEEE Trans Med Imag 1994;13:601–9.
14. Boccacci P, Bonetto P, Calvini P, Formiconi AR. A simple model for the the efficient correction of collimator blur in 3D SPECT imaging. Inverse Problems 1999;15:907–30.
15. Gelb DJ, Oliver E, Gilman S. Diagnostic criteria for Parkinson's disease. Arch Neurol 1999;56:33–9.

16. Deuschl G, Bain P, Brin M; Ad Hoc Scientific Committee. Consensus statement of the Movement Disorder Society on tremor. Mov Disord 1998;13(suppl 3):2–23.
17. Tatsch K, Asenbaum S, Bartenstein P, Catafau A, Halldin C, Pilowsky LS, et al. European Association of Nuclear Medicine procedure guidelines for brain neurotransmission SPET using ^{123}I-labelled dopamine D2 receptor ligands. Eur J Nucl Med Mol Imaging 2002;29:BP23–9.
18. Hamann C, Koch W, Radau PE, Tatsch K. Iterative reconstruction or filtered backprojection for quantitative assessment of dopamine d2 receptor studies? J Nucl Med 2003;44:114P.
19. Koch W, Radau PE, Münzing W, Tatsch K. Cross-camera comparison of SPECT measurements of a 3-D anthropomorphic basal ganglia phantom. Eur J Nucl Med Mol Imaging 2006;33:495–502.
20. Soret M, Koulibaly PM, Darcourt J, Hapdey S, Buvat I. Quantitative accuracy of dopaminergic neurotransmission imaging with ^{123}I SPECT. J Nucl Med 2003;44:1184–93.
21. Soret M, Koulibaly PM, Darcourt J, Buvat I. Partial volume effect correction in SPECT for striatal uptake measurements in patients with neurodegenerative diseases: impact upon patient classification. Eur J Nucl Med Mol Imaging 2006;33:1062–72.
22. Ogawa K, Harata Y, Ichihara T, Kubo A, Hashimoto N. A practical method for position-dependent Compton-scattered correction in single photon emission. IEEE Trans Med Imaging 1991;10:408–12.
23. Dallal GE. The little handbook of statistical practice. http://www.tufts.edu/~gdallal/LHSP.HTM at the page http://www.tufts.edu/~gdallal/corr.htm
24. Seibyl JP, Marek KL, Quinlan D, Sheff K, Zoghbi S, Zea-Ponce Y, et al. Decreased single-photon emission computed tomographic [^{123}I]beta-CIT striatal uptake correlates with symptom severity in Parkinson's disease. Ann Neurol 1995;38:589–98.
25. Carmack PS, Spence J, Gunst RF, Schucany WR, Woodward WA, Haleyb RW. Improved agreement between Talairach and MNI coordinate spaces in deep brain regions. NeuroImage 2004;22:367–71.
26. Colloby SJ, O'Brien JT, Fenwick JD, Firbank MJ, Burn DJ, McKeith IG, et al. The application of statistical parametric mapping to ^{123}I-FP-CIT SPECT in dementia with Lewy bodies, Alzheimer's disease and Parkinson's disease. NeuroImage 2004;23:956–66.
27. Van Laere K, Koole M, D'Asseler Y, Versijpt J, Audenaert K, Dumont F, et al. Automated stereotactic standardization of brain SPECT receptor data using single-photon transmission images. J Nucl Med 2001;42:361–75.
28. Lucignani G, Gobbo C, Moresco RM, Antonini A, Panzacchi A, Bonaldi L, et al. The feasibility of statistical parametric mapping for the analysis of positron emission tomography studies using ^{11}C-2-beta-carbomethoxy-3-beta-(4-fluorophenyl)-tropane in patients with movement disorders. Nucl Med Commun 2002;23:1047–55.